BMB Reports - Manuscript Submission

Manuscript Draft

DOI: 10.5483/BMBRep.2022-0170

Manuscript Number: BMB-22-170

Title: Cytosolic domain regulates the calcium sensitivity and surface expression of BEST1 channels in the HEK293 cells

Article Type: Article

Keywords: Bestrophin; Ca2+-dependent activation; Whole-cell recording; functional modulation; surface expression

Corresponding Author: Hyun-Ho Lim

Authors: Kwon Woo Kim[1,#], Junmo Hwang[1,#], Dong-Hyun Kim[1], Hyungju Park[1], Hyun-Ho Lim[1,2,*]

Institution: [1]Neurovascular Research Group, Korea Brain Research Institute (KBRI),
[2]Department of Brain Sciences, Daegu Gyeongbuk Institute of Science & Technology (DGIST),

Manuscript Type: Article

Cytosolic domain regulates the calcium sensitivity and surface expression of BEST1 channels in the HEK293 cells

Kwon Woo Kim[1†], Junmo Hwang[1†], Dong-Hyun Kim[1&], Hyungju Park[1,2] and Hyun-Ho Lim[1,2*]

[1]Neurovascular Research Group, Korea Brain Research Institute (KBRI), Daegu, 41068, Republic of Korea, [2]Department of Brain Sciences, Daegu Gyeongbuk Institute of Science & Technology (DGIST), Daegu, 42988, Republic of Korea

[†]These authors were equally contributed to this work.

[&]Present address: Quantum Design Korea, Seoul, 06272, Republic of Korea

Running Title: C-terminal regulation of Bestrophin1 channel

Keywords: Bestrophin, Ca^{2+}-dependent activation, Whole-cell recording, functional modulation, surface expression

[*]**Corresponding Author's Information:**
Hyun-Ho Lim, Ph.D.
Laboratory of Molecular Physiology and Biophysics
Neurovascular Unit Research Group, Korea Brain Research Institute
61 Cheomdan-ro, Dong-gu, Daegu, 41068, Republic of Korea
hhlim@kbri.re.kr, +82-53-980-8330

ABSTRACT

BEST family is a class of Ca^{2+}-activated Cl^- channels evolutionary well conserved from bacteria to human. The human BEST paralogs (BEST1 – BEST4) share significant amino acid sequence homology in the N-terminal region, which forms the transmembrane helicases and contains the direct calcium-binding site, Ca^{2+}-clasp. But the cytosolic C-terminal region is less conserved in the paralogs. Interestingly, this domain-specific sequence conservation is also found in the BEST1 orthologs. However, the functional role of the C-terminal region in the BEST channels is still poorly understood. Thus, we aimed to understand the functional role of the C-terminal region in the human and mouse BEST1 channels by using electrophysiological recordings. We found that the calcium-dependent activation of BEST1 channels can be modulated by the C-terminal region. The C-terminal deletion hBEST1 reduced the Ca^{2+}-dependent current activation and the hBEST1-mBEST1 chimera showed a significantly reduced calcium sensitivity to hBEST1 in the HEK293 cells. And the C-terminal domain could regulate cellular expression and plasma membrane targeting of BEST1 channels. Our results can provide a basis for understanding the C-terminal roles in the structure-function of BEST family proteins.

INTRODUCTION

Bestrophin (BEST) channels are a class of calcium-activated Cl^- channels, which are activated by a cytoplasmic [Ca^{2+}] increase (1). The BEST1 channel was initially identified by the linkage analysis of the eye disease, Bestrophin vitelliform macular dystrophy (BVMD). Thereafter four BEST channel paralogs (BEST1 to BEST4) have been found in the human genome and the BEST channels have been found in virtually all living organisms from bacteria to human (1, 2). Although the mutations in BEST1 channel produced retinopathy, the pathophysiological role of BEST1 channel is not clear (1, 3). Interestingly, a series of seminal works from Justin C. Lee's group showed that BEST1 channels, expressed in the mouse astrocytes, secrete gliotransmitters including glutamate, GABA, and D-serine, which can modulate neuronal activities in the tripartite synapse (4-6).

Human BEST channel paralogs (hBEST1~hBEST4) share ~60% sequence identity in the N-terminal ~370 amino acids but retain 6~19% sequence identity in the remaining C-terminal region. Similarly, the distinct sequence identities between human and mouse BEST1 ortholog are also present (7). Although four human paralogs share significant sequence identity in the N-terminal region, the electrophysiological recordings showed different current-voltage (I-V) characteristics of BEST paralogs: The hBEST1 produces instantaneous slightly outward-rectifying current, the hBEST2 shows linear I-V relationship, the hBEST3 has time-dependently activated current with strong inward rectification, and the hBEST4 produces linear I-V curve with time-dependent inactivation (7, 8). These functional diversities of BEST paralogs imply that the marginally conserved C-terminal domain could modulate the BEST paralogs differentially. Indeed, the electrophysiological studies suggested that the autoinhibitory domain is localized in the cytosolic C-terminal domain of BEST3 (AID). And the AID was also found in the BEST2, but its action could be antagonized by the facilitatory domain (9, 10).

Structural studies have revealed the three-dimensional architectures of several BEST channel homologs including chicken BEST1 (cBEST1) (11, 12), bovine BEST2 (bBEST2) (13), hBEST1, and hBEST2 (14). The structures showed that the functional BESTs are formed by the homo-pentameric assembly. Also, several important regions of the BEST channels were revealed by the structures. First, the BEST structures showed that the conserved acid patch forms the direct calcium-binding site (Ca^{2+}-clasp). Second, the anion conduction pore in BEST channels has two physical constriction zones. The Neck is formed by the pore-lining hydrophobic residues (^{76}Ile, ^{80}Phe, ^{84}Phe) and the aperture is formed by the nonpolar residue

(^{205}Ile in hBEST1). Third, the auto-inhibitory segment (AS, residue 346~378 in hBEST1) wraps the periphery of the BEST channel cytosolic domain in the closed state, but the detachment of AS may facilitate channel opening (14). However, none of the BEST channel structures visualized the C-terminal domain beyond amino acid residue 379. The structures of cBEST1 and bBEST2 were determined by using the C-terminal truncated proteins ($cBEST1_{1-405}$, $cBEST1_{1-345}$, or $bBEST2_{1-406}$; the numbers indicate the amino acid residues used in the structural studies) for the easy of structural determination (11-13). However, the full-length hBEST1 and hBEST2 structures also failed to resolve the C-terminal structure (14), which might be due to the disordered C-terminal domain in the cryo-EM conditions or intrinsically disordered nature of it. Thus, the structural role of the cytosolic C-terminal domain remains elusive.

In this study, we aimed to understand the functional roles of the BEST1 channel's C-terminal domain by the electrophysiological characterizations of human and mouse orthologs. We found that the expression and Ca^{2+}-dependent activation of hBEST1 differ from those of mBEST1 despite having identical calcium-binding sites. Interestingly, deletion of C-terminal 218 residues in hBEST1 significantly reduced Ca^{2+}-dependent current activation though total and surface expressions were not significantly reduced. The replacement of hBEST1 C-terminal region with mBEST1 (hBEST1-mBEST1 chimeric channel) resulted in a 15-fold reduced calcium sensitivity to hBEST1. However, the functionality of mBEST1-hBEST1 chimera were barely observed, though the expression level was significantly increase to mBEST1. These results indicate that the calcium-dependent activation of BEST1 channels could be determined by the direct calcium binding to the Ca^{2+}-clasp in N-terminal region as well as the modulatory function of C-terminal region. Also, the C-terminal domain could regulate the cellular expression and plasma membrane targeting of BEST1 channels.

RESULTS

The amino acid sequence identities among BEST1 channel orthologs are separable in two regions: The highly homologous N-region (residues 1~367), which shares 74.9~99.2% identities, and the marginally homologous C-region (residue 368~end) having 35.2~92.7% identities (Fig. 1A, Fig. S1). Are these marginal conserved and structurally disordered C-region simply tethered to the BEST1 channel core? However, the previous study suggested that the facilitatory domain (residue 405~454) has an active role in the mouse BEST2 channel (9). Also, several hBEST1 mutations in the C-region are known to link to retinopathy (15). These pathogenic hBEST1 variants imply that the C-region is not merely attached to the BEST1 channel core. Thus, we wondered what the functional role of the C-region in BEST1 channel activation is.

Ca^{2+}-dependent activations and expression of hBEST1 and mBEST1 are different

The activities of hBEST1 and mBEST1 were examined by using whole-cell patch clamp experiments with various $[Ca^{2+}]_i$. To avoid any unexpected effect on the electrophysiological characteristics of BEST1 channels, we have used the BEST1 channel coding sequences without any protein tag. The hBEST1 channels expressed in HEK293T cells generated slightly outward rectifying Cl^- currents in response to the intracellular calcium (Fig. 1B). The hBEST1 channels began to be activated at 100 nM $[Ca^{2+}]_i$ and reached the maximal activation at 300 nM $[Ca^{2+}]_i$ with the half-maximal activation $[Ca^{2+}]_i$ (EC_{50}) of ~174 nM and the Hill coefficient of ~3.7 (5~15 observations for each $[Ca^{2+}]_i$). But the *mBEST1* transfected cells did not show any $[Ca^{2+}]_i$-dependent current even in the presence of 100 mM $[Ca^{2+}]_i$, more than 500-fold excess of hBEST1's EC_{50} (Fig. 1E~G). The current densities at +60 mV were 38.3 ± 8.0 pA/pF for hBEST1 (1 mM $[Ca^{2+}]_i$, n = 15) and 6.9 ± 1.4 pA/pF for mBEST1 (100 mM $[Ca^{2+}]_i$, n = 3). The current density level of *mBEST1* transfected cells was indistinguishable to the untransfected cells.

To investigate whether the low current density of the *mBEST1* transfected cells was due to the low protein expression level, reduced membrane surface expression, or functional impairment of mBEST1 channel, the surface biotinylated HEK293T cells expressing each BEST1 construct were subjected to the western blot analysis to quantify the total expression levels and cell surface targeted fractions as previously described (16) (Fig. 2). For this purpose, we used *BEST1* genes in-frame fused with C-terminal Flag tag to detect both hBEST1 and mBEST1 proteins simultaneously. Surprisingly, the total and surface expressions of mBEST1

were not detectable (Fig. 2). However, the C-region (residue 368~551) deleted mBEST1 ($mBEST1_{367}$) was expressed in HEK293T cells and the expression level was 22.5 ± 2.9 % (n = 4) of hBEST1, albeit the surface expression was not detectable (Fig. 2). To test whether these distinct expression levels of the hBEST1 and mBEST1 can be replicated in the murine cell lines, the expression of hBEST1 and mBEST1 tagged with either N-terminal or C-terminal protein tag (Flag, BRIL-twin strep, or BRIL-3X Flag) was examined in CHO-K1 cells. The BRIL tag (~10kDa) was originated from the thermostabilized mutant apocytochrome b_{562}RIL, which have been widely used for stabilizing various membrane proteins including the GPCR (17). The expression level of N-terminal Flag tagged hBEST1 (Flag-hBEST1) was significantly lower than other C-terminal tagged or untagged hBEST1. However, the expression level hBEST1-Flag driven by either CMV or CAG promoter was not significantly different (Fig. S2A and B). Interestingly, the mBEST1 with C-terminal BRIL-3X Flag tag was expressed well but the N- or C-terminal Flag tagged mBEST1 was not expressed at all in the CHO-K1 cells. These results indicate that the C-region can regulate the expression and membrane targeting of BEST1 channels and the expression of mBEST1 can be stabilized with a large C-terminal tag.

The C-terminal domain regulates the Ca^{2+}-dependent gating of hBEST1

To investigate the role of C-region in the $[Ca^{2+}]_i$-sensitivity of BEST1 channels, we examined the effect of the C-region deletions on the hBEST1 currents (Fig. 3A). First, the functional consequences of $hBEST1_{345}$ ($hBEST1_{1\text{-}345}$) mutant, which encodes only transmembrane core domain (14), were accessed by the electrophysiological recordings. The $hBEST1_{345}$ showed robust $[Ca^{2+}]_i$-dependent currents with the EC_{50} of ~470 nM (3~8 observations), which differs less than an order of magnitude (~2.5-fold decrease) to wildtype hBEST1. The current density of $hBEST1_{345}$ was slightly larger than wildtype hBEST1 (Fig. 3B and C, *green*). However, the cooperativity of $[Ca^{2+}]_i$-dependency became shallower: the Hill coefficient for the $[Ca^{2+}]_i$-dependent gating of $hBEST1_{345}$ is ~1.5 (Fig. 3D, *green*).

Another truncated mutant $hBEST1_{367}$ ($hBEST1_{1\text{-}367}$), which spans the highly conserved N-region (Fig. 2A, Fig. 1A, and Fig. S1), resulted in a very low level of $[Ca^{2+}]_i$-dependent currents with the maximum current density of 12.0 ± 2.6 pA/pF at +60 mV in the presence of 10 mM $[Ca^{2+}]_i$. The EC_{50} and Hill coefficient are ~470 nM and ~1.8, respectively (3~4 observations). However, the total protein expression and surface expression level of $hBEST1_{367}$ are not significantly different from those of wildtype hBEST1 (Fig. 2). These results suggested

that the C-region (residue 368~585) deletion of hBEST1 could perturb the $[Ca^{2+}]_i$-dependent gating of hBEST1 without affecting protein expression and membrane targeting.

The C-region swapped mutant, hmBEST1 has an altered Ca^{2+}-sensitivity

Next, we examined the electrophysiological activities of C-domain swap constructs of hmBEST1($hBEST1_{1-367}$—$mBEST1_{368-551}$) and mhBEST1 ($mBEST1_{1-367}$—$hBEST1_{368-585}$) (Fig. 4). The hmBEST1 showed ~2-fold increased current density (86.7 ± 23.6 pA/pF at +60 mV in the presence of 10 mM $[Ca^{2+}]_i$) to wildtype hBEST1, but the mhBEST1 chimera did not evoke the $[Ca^{2+}]_i$-dependent currents (Fig. 4A~F). The hmBEST1 channels were activated by $[Ca^{2+}]_i$ with the EC_{50} of ~3.1 mM and the Hill coefficient of ~4.3 (3~5 observations for each $[Ca^{2+}]_i$) (Fig. 4C). Interestingly, the Ca^{2+}-sensitivity of hmBEST1 was reduced by ~18-fold compared to wildtype hBEST1 without significantly changing the $[Ca^{2+}]$ cooperativity.

The C-terminal region regulates the Ca^{2+}-dependent run-up and run-down of BEST1 channels

The effect of C-terminal region on the time-dependent whole-cell current generations was examined. The hBEST1 currents reached the maximum level in 67.1 ± 25.0 s at +100 mV in 10 mM $[Ca^{2+}]_i$ (n = 5) and then began to be inactivated with the half-maximum time (T_{50}) of 176.1 ± 28.4 s (n = 5) (Fig. 4G). However, the $hBEST1_{345}$ took more time for full activation (201.3 ± 32.1 s at +100 mV in 10 mM $[Ca^{2+}]_i$ (n = 7)) and the current level was persisted without run-down (Fig. 4H). Previously, the C-terminal deletion mutant $hBEST1_{380}$ ($hBEST1_{1-380}$) showed a similar whole-cell current kinetics to $hBEST1_{345}$, but other deletion mutants, $hBEST1_{350}$, $hBEST1_{360}$, and $hBEST1_{370}$ were essentially nonfunctional (18). The hmBEST1 chimera showed accelerated run-up (53.5 ± 16.3 s at +100 mV in the presence of 10 mM $[Ca^{2+}]_i$ (n = 3)) and slowed run-down (Fig. 4I). These results implied that the BEST1 C-terminal region (residue 346~end) can regulate both the Ca^{2+}-dependent run-up and run-down of BEST1 channel.

As seen in Fig. 2, the total expression levels of hmBEST1 and mhBEST1 were 14.4 ± 4.6 % (n=4) and 51.5 ± 6.0 % (n=4) of hBEST1 level, respectively. And the relative surface expression levels were 17.0 ± 7.2 % (n=4) and 4.7 ± 0.8 % (n=4) of hBEST1 level, respectively. The results of increased current density but the reduced surface expression of hmBEST1 to wildtype hBEST1 are somewhat counterintuitive. Though we do not have direct experimental evidence for making an explanation, it is possible that the C-region has an inhibitory function

for BEST1 channel opening in a species-specific manner. The removed run-down of $hBEST1_{345}$ and the slowed run-down of hmBEST1 chimera could partly support the idea (Fig. 4H~I). These results supported that the C-region could regulate the total and membrane surface expression of BEST1 channels as well as modulate channel functions.

DISCUSSION

In summary, we found that BEST1 orthologs, C-terminal deletions, and C-region swapped BEST1 sense intracellular calcium with different EC_{50} values and cooperativities. And these differences could be attributed to the modulatory effect of the marginally homologous C-region. Also, we found that the C-regions can regulate the expression and membrane targeting of BEST1 channels. We believe that these data provide insight to understand the functional role of marginally conserved C-regions among the BEST1 homologs on the Ca^{2+}-dependent gating.

The low-level current density of $hBEST1_{367}$ is well-matched to the previous work of the Hartzell group, where the C-truncated hBEST1 channels (residues 1-350, 1-360, and 1-370) were essentially non-functional (18) (Fig. 3). However, the recent work done in the Yang lab. showed that the $hBEST1_{1\text{-}367}$ and $hBEST2_{1\text{-}368}$ channels could produce larger current densities than parental wildtype channels even in the absence of Ca^{2+} (14). One plausible explanation for this obvious discrepancy may come from the different compositions of pipette (intracellular) solution during whole-cell patch-clamp recordings, especially whether it included ATP or not. Since it had been suggested that ATP can activate the BEST channels through direct binding to the cytosolic loop (residue 199~203 in hBEST1) (19), we did not include ATP in our pipette solution to rule out any effect to activate BEST1 channels other than $[Ca^{2+}]_i$. However, we do not have any experimental data for supporting this possibility at this moment. Another possibility might be due to the presence of C-terminal tag used in the previous study (14), in which all the C-terminally truncated hBEST1 and hBEST2 constructs were fused with the C-terminal YFP protein. It will be interesting to compare the functional characteristics of BEST1 channels with various protein tags.

In the previous study, the mBEST1 was expressed in the TRex-293 cells with a tetracycline inducible expression system of pcDNA4/TO/c-myc-HIS vector, where the mBEST1 cDNA was in-frame fused with the C-terminal c-myc and 6X His tags in tandem (~20 amino acids long) (20). Counterintuitively, the mBEST1 with N- or C-terminal Flag-tag (8

amino acids long) was not expressed at all both in the HEK293 and CHO-K1 cells (Fig. 2 and Fig. S2C). However, the mBEST1 with a large C-terminal tandem tag (BRIL-3X Flag) was effectively expressed in CHO-K1 cells (Fig. S2C). This result indicates that the presence of large C-terminal tags may stabilize the expression of mBEST1 in the heterologous expression systems.

How does the C-region regulate the Ca^{2+}-sensitivity on the BEST1 channel? The previous work showed that the deletion or neutralization mutations of a potential Ca^{2+}-binding site (^{380}EDEED^{384}) in the C-region did not have any effect on the Ca^{2+}-dependent activation. And the C-truncated mutant hBEST1$_{390}$ had a wildtype-like activity (18). However, the D312G mutant hBEST1 was ~20-fold less sensitive to Ca^{2+} with the EC_{50} of 2.7 mM and lost cooperative Ca^{2+}-binding (18). Thus, the reduced Ca^{2+}-sensitivity in hmBEST1 is likely due to the failure of modulation by the mBEST1's C-region, though we do not have any experimental evidence for ruling out the existence of another Ca^{2+}-binding site(s) in the BEST1's C-region. Nonetheless, our results indicated that the calcium-dependent activation of BEST1 channels is a result of the concerted action of the direct calcium binding to Ca^{2+}-clasp in the N-region and the modulatory action of C-region.

Our results showed that the mBEST1 was not expressed in the HEK293T cells, but the C-region deletion mutant mBEST1$_{367}$ and the chimeric mhBEST1 were expressed though their membrane localizations were largely impaired. And the expression level and surface targeting of hBEST1 with mBEST's C-region (hmBEST1) were also reduced (Fig. 2). Thus, the C-region of mBEST1 somehow hinders the expression and the N-region is important to membrane targeting of BEST1. It will be interesting to explore whether BEST1's domain itself or any auxiliary partner regulates this intriguing ortholog-dependent expression.

MATERIALS AND METHODS

The cells, culture media, antibodies, biochemical reagents used in this work are listed in the supplementary information (Table S1).

Methods for the plasmid DNA construction, cell culture, transfection, electrophysiological recording, cell surface biotinylation, and western blot analysis are described in the supplementary information (Supplementary Methods).

ACKNOWLEDGMENTS

We thank the members of the Lim laboratory for their timely help throughout the study. This work was supported by the Basic Science Research Program through the National Research Foundation of Korea (NRF) grants (2021R1A2C1004884 to H.-H.L.) and the Brain Research Program of the NRF (2020M3E5D9079 to H.-H.L.) funded by the Ministry of Science and ICT, Republic of Korea, and the KBRI basic research program through Korea Brain Research Institute funded by the Ministry of Science and ICT (22-BR-01-02 to H.-H.L.).

CONFLICTS OF INTEREST

The authors declare no conflict of interest.

FIGURE LEGENDS

Fig. 1. Ca^{2+}-dependent activation of hBEST1 and mBEST1. A. schematic drawing of BEST1 channels domain architecture (*left*) and amino acid sequence identities of BEST1 orthologs to hBEST1 (*right*). The UniProt accession numbers of BEST1 orthologs are O76090 (human), Q6UY87 (monkey), Q6AYG9 (rat), O88870 (mouse), and E1C3A0 (chicken). Representative whole-cell current traces of hBEST1 (B) and mBEST1 (E) activated by indicated $[Ca^{2+}]_i$. The currents were evoked by 1-s step pulses from -100 mV to +100 mV with 20 mV increments (B, *left*). The representative current of untransfected cell was drawn in gray (E, *left*). The dashed lines in the current traces indicate the zero-current levels throughout the remaining figures. The current-voltage ($I_{density}$-V) relationships of hBEST1 (C) and mBEST1 (F) in the various $[Ca^{2+}]_i$. Symbols represent the steady state mean current ± standard error of the mean (s.e.m.) (n = 3~15). The $I_{density}$-V relationship of untransfected cells in 1 mM $[Ca^{2+}]_i$ is in gray. The $[Ca^{2+}]_i$-dependent activation curves of hBEST1 (D) and mBEST1 (G) at +60 mV. Gray symbols represent the $I_{density}$ of untransfected cells. Dose-response current increases of hBEST1 were fitted with Hill equation.

Fig. 2. Total and cell surface expression of wildtype, C-terminal truncated, and chimeric BEST1 channels. Representative western blot images of total protein expression and cell surface expression of various BEST1 constructs with C-terminal Flag tag expressed in HEK293T cells. Quantification of total protein expression level normalized to the density of actin (B) and relative surface expression level to the total expression level (C). Data (mean ± s.e.m.) were produced by four independent transfections. Empty circles in the bar graphs indicate the values from the independent observations. One-Way ANOVA test was used for comparisons, and the appropriate P values are indicated in each graph.

Fig. 3. Ionic currents through the C-terminal truncated hBEST1 channels. A. schematic drawing of the C-terminal truncated $hBEST1_{345}$ and $hBEST1_{367}$. B. Representative whole-cell current traces of $hBEST1_{345}$ (*green*) and $hBEST1_{367}$ (*red*) activated by indicated $[Ca^{2+}]_i$. C. The $I_{density}$-V relationships of $hBEST1_{345}$ (*green*) and $hBEST1_{367}$ (*red*) in the various $[Ca^{2+}]_i$. Symbols represent the mean ± s.e.m. (n = 3~8). D. the $[Ca^{2+}]_i$-dependent activation curves of $hBEST1_{345}$ (*green*) and $hBEST1_{367}$ (*red*) at +60 mV. Dose-response current increases of hBEST1 were fitted with Hill equation. Dashed gray curve represents the fitted $[Ca^{2+}]_i$-response of wildtype hBEST1 (as in Fig. 1D).

Fig. 4. Ca^{2+}-dependent activation of C-terminal swapped hBEST1 and mBEST1. Schematic drawing of the domain-swapped hmBEST1 ($hBEST1_{1-367}$—$mBEST1_{368-551}$) (A) and mhBEST1 ($mBEST1_{1-367}$—$hBEST1_{368-585}$) channels (D). Representative whole-cell current traces of hmBEST1 (A) and mhBEST1 (D) activated with indicated $[Ca^{2+}]_i$. The current density-voltage ($I_{density}$-V) relationships and the $[Ca^{2+}]_i$-dependent activation curves of hmBEST1 (B and C, respectively) and mhBEST1 (E and F, respectively) in the various $[Ca^{2+}]_i$. Dashed gray curve represents the fitted $[Ca^{2+}]_i$-response of wildtype hBEST1 (as in Fig. 1D). Run-up and run-down time courses of hBEST1 (G), $hBEST1_{345}$, and (H) hmBEST1 channels. The time zero represents the time point of first voltage stimulation immediately after making whole-cell configuration. The currents were evoked by the 1-s stimulation of +100 mV followed by 1-s stimulation of -100 mV in every 10 s. Each symbol represents steady state current at +100 mV (outward current) or -100 mV (inward current) in the presence of the indicated $[Ca^{2+}]_i$. The T_{max} is the time for reaching the maximum current value at +100 mV (G, H, and I) and the $T_{50,\ inactivation}$ is the time for reaching the 50% value of maximum current from the maximum level (G). The bar graphs represent the mean ± s.e.m. (n = 3~8). *Black* circles in the bar graphs indicate the values from the independent observations.

REFERENCES

1. Hartzell HC, Qu Z, Yu K, Xiao Q and Chien LT (2008) Molecular physiology of bestrophins: multifunctional membrane proteins linked to best disease and other retinopathies. Physiol Rev 88, 639-672
2. Hagen AR, Barabote RD and Saier MH (2005) The bestrophin family of anion channels: identification of prokaryotic homologues. Mol Membr Biol 22, 291-302
3. Owji AP, Kittredge A, Zhang Y and Yang T (2021) Structure and Function of the Bestrophin family of calcium-activated chloride channels. Channels (Austin) 15, 604-623
4. Woo DH, Han KS, Shim JW et al (2012) TREK-1 and Best1 channels mediate fast and slow glutamate release in astrocytes upon GPCR activation. Cell 151, 25-40
5. Jo S, Yarishkin O, Hwang YJ et al (2014) GABA from reactive astrocytes impairs memory in mouse models of Alzheimer's disease. Nat Med 20, 886-896
6. Koh W, Park M, Chun YE et al (2022) Astrocytes Render Memory Flexible by Releasing D-Serine and Regulating NMDA Receptor Tone in the Hippocampus. Biol Psychiatry 91, 740-752
7. Tsunenari T, Sun H, Williams J et al (2003) Structure-function analysis of the bestrophin family of anion channels. J Biol Chem 278, 41114-41125
8. Sun H, Tsunenari T, Yau KW and Nathans J (2002) The vitelliform macular dystrophy protein defines a new family of chloride channels. Proc Natl Acad Sci U S A 99, 4008-4013
9. Qu Z, Cui Y and Hartzell C (2006) A short motif in the C-terminus of mouse bestrophin 3 [corrected] inhibits its activation as a Cl channel. FEBS Lett 580, 2141-2146
10. Qu ZQ, Yu K, Cui YY, Ying C and Hartzell C (2007) Activation of bestrophin Cl-channels is regulated by C-terminal domains. J Biol Chem 282, 17460-17467
11. Kane Dickson V, Pedi L and Long SB (2014) Structure and insights into the function of a Ca(2+)-activated Cl(-) channel. Nature 516, 213-218
12. Miller AN, Vaisey G and Long SB (2019) Molecular mechanisms of gating in the calcium-activated chloride channel bestrophin. Elife 8
13. Owji AP, Zhao Q, Ji C et al (2020) Structural and functional characterization of the bestrophin-2 anion channel. Nat Struct Mol Biol 27, 382-391
14. Owji AP, Wang J, Kittredge A et al (2022) Structures and gating mechanisms of human

bestrophin anion channels. Nat Commun 13, 3836

15. Simonyan V, Chumakov K, Dingerdissen H et al (2016) High-performance integrated virtual environment (HIVE): a robust infrastructure for next-generation sequence data analysis. Database (Oxford) 2016
16. Hwang J, Park K, Lee GY et al (2021) Transmembrane topology and oligomeric nature of an astrocytic membrane protein, MLC1. Open Biol 11, 210103
17. Chun E, Thompson AA, Liu W et al (2012) Fusion partner toolchest for the stabilization and crystallization of G protein-coupled receptors. Structure 20, 967-976
18. Xiao Q, Prussia A, Yu K, Cui YY and Hartzell HC (2008) Regulation of bestrophin Cl channels by calcium: role of the C terminus. J Gen Physiol 132, 681-692
19. Zhang Y, Kittredge A, Ward N, Ji C, Chen S and Yang T (2018) ATP activates bestrophin ion channels through direct interaction. Nat Commun 9, 3126
20. O'Driscoll KE, Leblanc N, Hatton WJ and Britton FC (2009) Functional properties of murine bestrophin 1 channel. Biochem Biophys Res Commun 384, 476-481

Kim et al., Fig.1

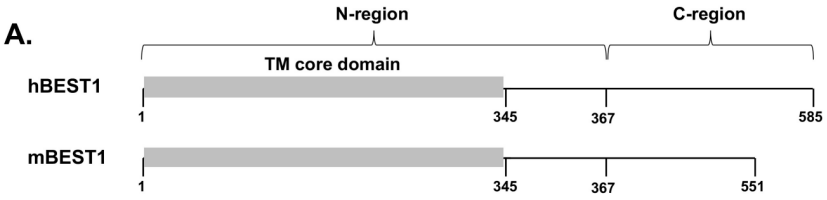

BEST1 orthologs	Sequence identity to hBEST1 (%)		
	Overall (1 - end)	N-region (1 - 367)	C-region (368 - end)
monkey	96.8	99.2	92.7
rat	68.1	81.2	39.2
mouse	67.8	82.8	36.4
chicken	60.0	74.9	35.2

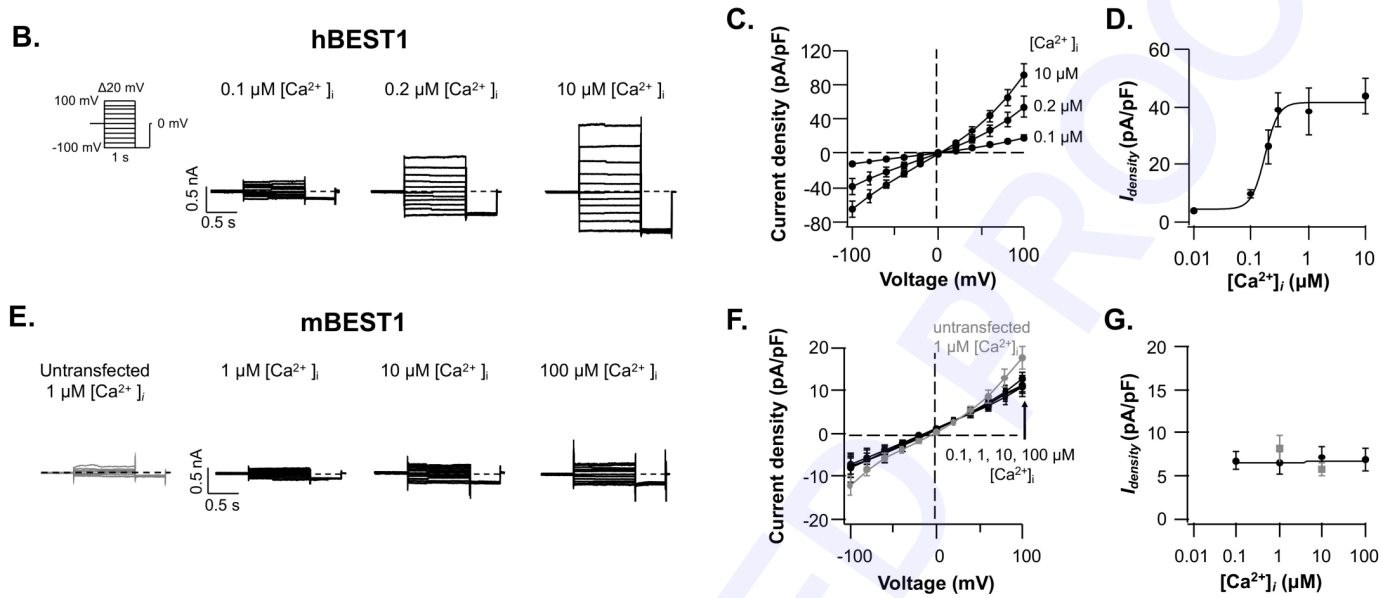

Fig. 1. Figure 1

Kim et al., Fig. 2

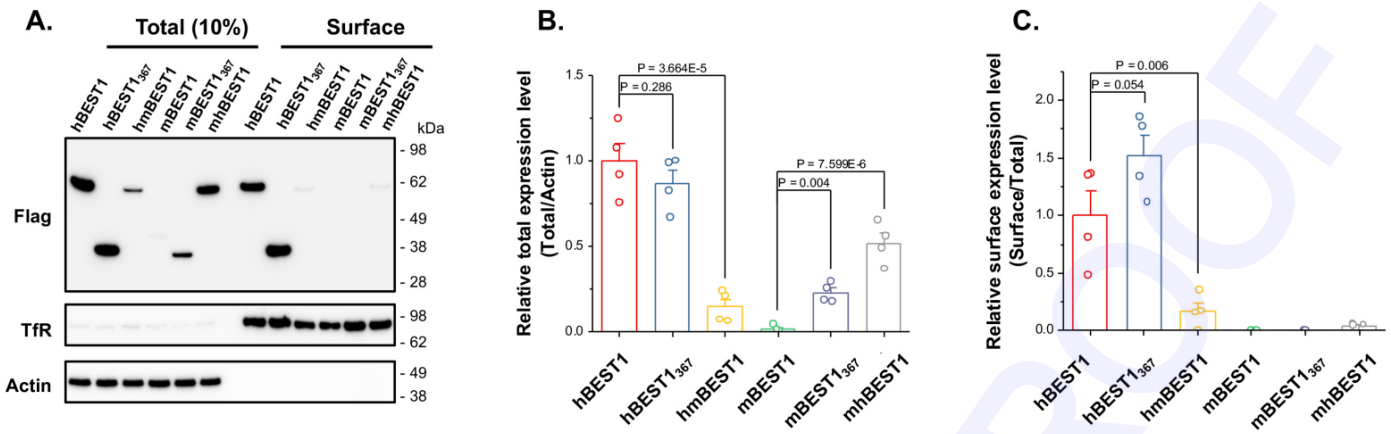

Fig. 2. Figure 2

Kim et al., Fig. 3

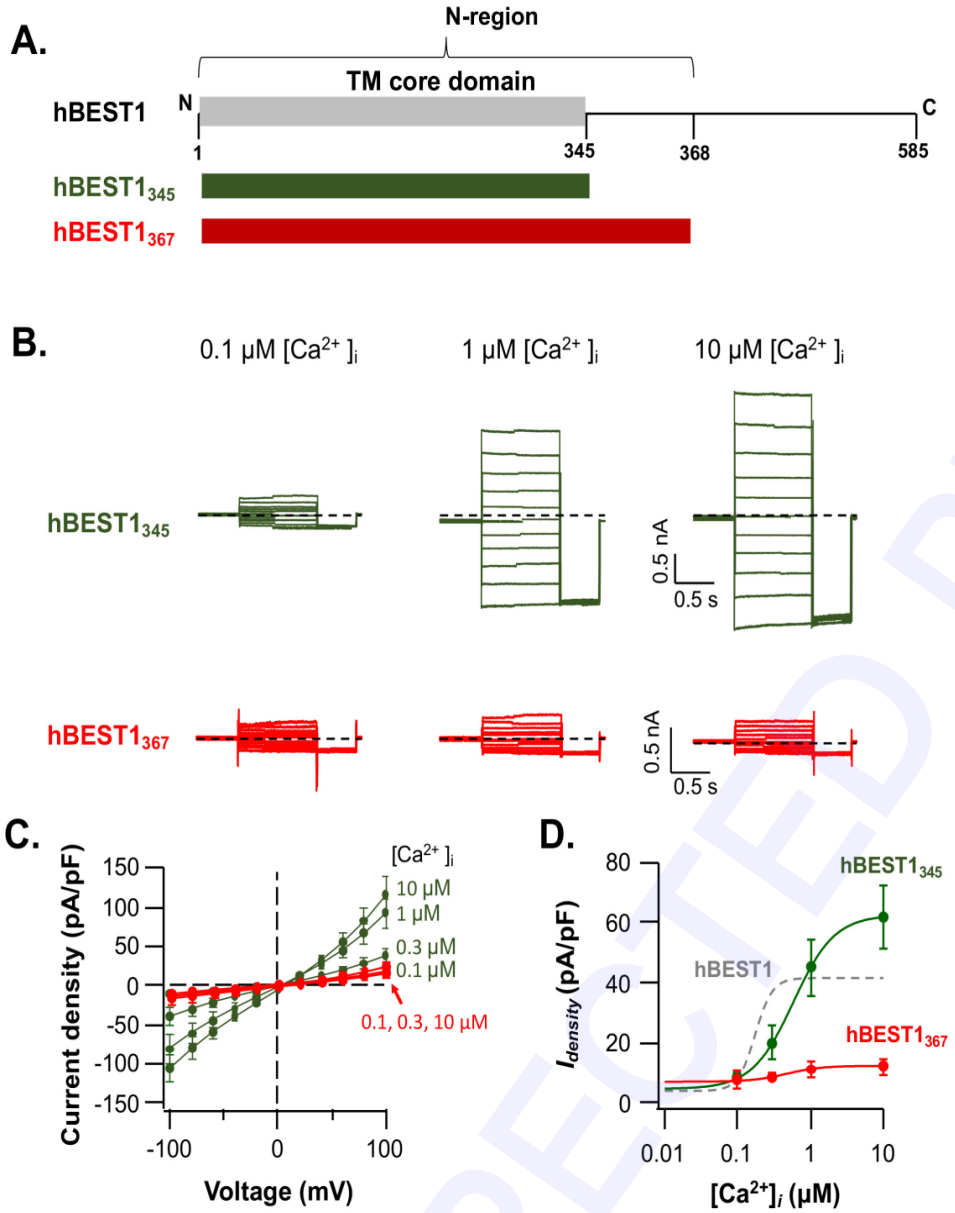

Fig. 3. Figure 3

Kim et al., Fig. 4

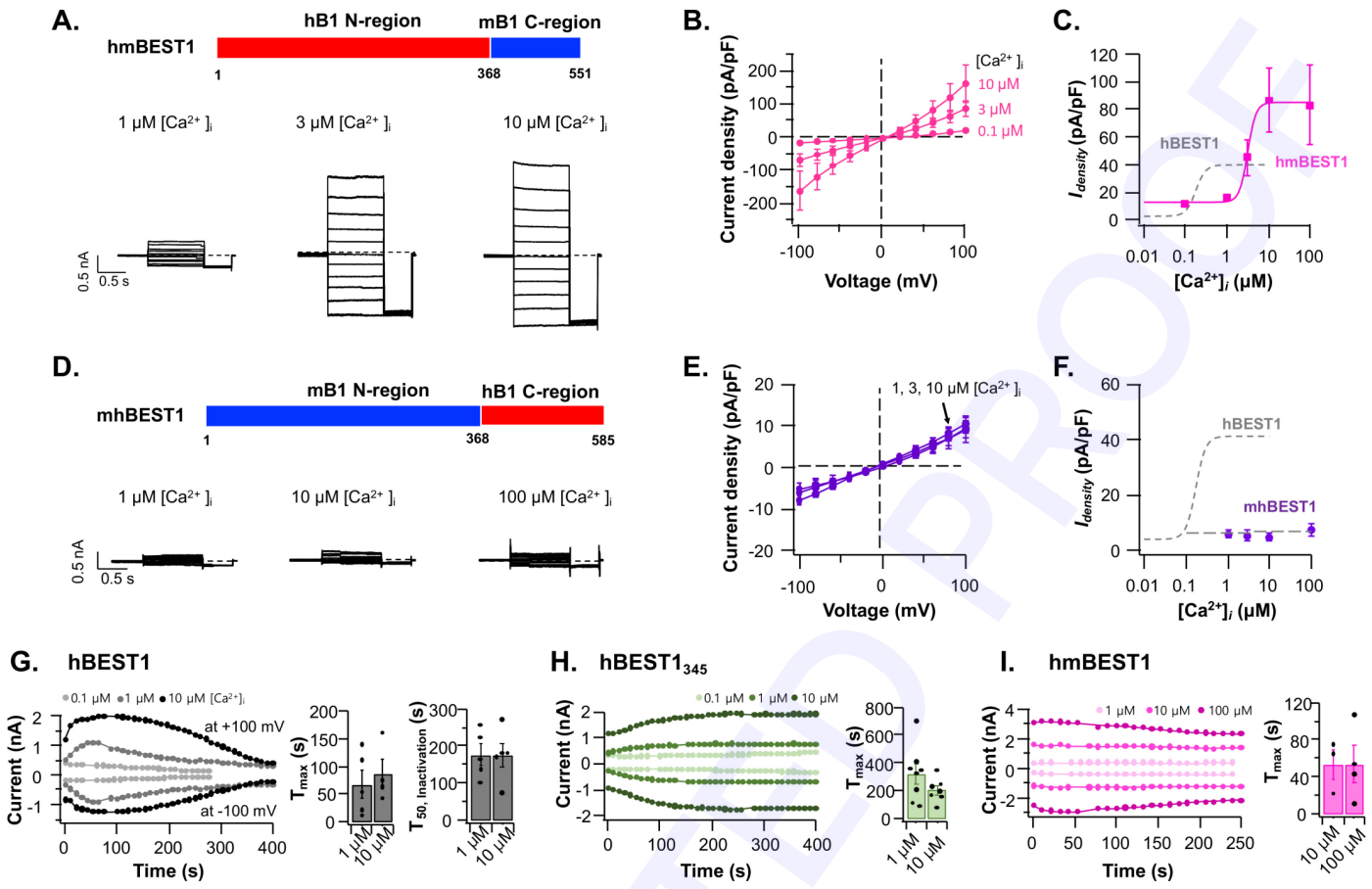

Fig. 4. Figure 4

Supplementary Information

Cytosolic domain regulates the calcium sensitivity and surface expression of BEST1 channels in the HEK293 cells

Kwon Woo Kim[1†], Junmo Hwang[1†], Dong-Hyun Kim[1&], Hyungju Park[1,2] and Hyun-Ho Lim[1,2*]

[1]Neurovascular Research Group, Korea Brain Research Institute (KBRI), Daegu, 41068, Republic of Korea, [2]Department of Brain Sciences, Daegu Gyeongbuk Institute of Science & Technology (DGIST), Daegu, 42988, Republic of Korea

[†]These authors were equally contributed to this work

Table S1. List of reagents

No	Item	Catalog no.	Manufacturer	Company's location
1	HEK293T cell	CRL-3216	ATCC	Manassas, VA
2	Anti-Flag M2 antibody	F1804, RRID:AB_262044	Sigma-Aldrich	St Louis, MO
3	Anti-Actin	8457S, RRID:AB_10950489	Cell Signaling	Danvers, MA
4	Anti-Bestrophin-1 (extracellular antibody)	ABC-001, RRID: AB_10560217	Alomone	Jerusalem, Israel
5	Anti-BEST1 antibody	Ab2182, RRID: AB_302880	Abcam	Cambridge, UK
6	Anti-Transferrin receptor antibody	ab84036, AB_10673794		
7	EZ-Link Sulfo-NHS-SS-Biotin	21331	Thermo Fisher Scientific	Waltham, MA
8	NeutrAvidin Plus UltraLink Resin	53151		
9	LDS sample buffer	B0007 and B0009		
10	Bolt™ 4-12% Bis-Tris Plus Gel	NW04120BOX		
11	iBlot 2 Transfer Stack	IB24001		
12	iBind Flex Solution	SLF2020		
13	Fetal bovine serum	FBS, 16000-044		
14	Dulbecco's modified Eagle's medium (DMEM)	11995073		
15	Opti-MEM	31985-062		
16	Clarity Western ECL Substrate	BR170-5061	Bio-Rad	Hercules, CA
17	Transporter 5 Transfection Reagent	26008-50	Polyscience	Warrington, PA

Supplementary Methods

Plasmid DNA construction, cell culture, and transfection

Human BEST1 (NM_004183.4) and mouse Best1 (NM_011913.2) were purchased from GenScript. For electrophysiological recordings, the coding sequences of full-length, C-terminal truncated, and domain-swapped hBEST1 or mBEST1 were subcloned into pEEV-CAG vector. In case of total and surface expression experiments, the coding sequences were in-frame fused with C-terminal Flag tag. All sequences were confirmed via the conventional sequencing method. The HEK293T cells were maintained in DMEM supplemented with 10% FBS and kept at 37°C in a humidified 5% CO_2 incubator. Subculture was performed every 2-3 days to maintain 80-90% confluency. For transfection, cells were seeded in culture plate and incubated for 24 hours to achieve 50-70% confluency. 1 μg plasmid DNA and 6 μg Transporter 5 Transfection Reagent were mixed in 0.1 mL Opti-MEM per 35 mm culture dish and incubated for 15 min at 23°C. For whole-cell patch-clamp recording, 0.1 μg GFP expression plasmid DNA was co-transfected for identifying transfected cells under fluorescence microscope. A day after transfection, the cells were detached by trypsin and plated onto the poly-L-lysine coated 5 mm × 5 mm coverslip chips.

Electrophysiological recording

Cells were recorded by whole-cell patch clamp configuration at room temperature (22~25°C). The patch pipettes were pulled from borosilicate glass micropipette capillaries using a P-1000 micropipette puller (Sutter Instrument) and fire-polished by using MF-900 microforge (Narishige) with resistances between 2~4 MΩ. Recordings were performed using an Axopatch 200B (Molecular Device) with pCLAMP 10.2 software (Molecular Device). The currents were sampled at 5 kHz using an Axon Digidata 1550B digitizer (Molecular Device) and filtered at 2 kHz with a lowpass Bessel filter. Series-resistance errors were compensated by 60% and fast and slow capacitance was compensated. The ionic current through the BEST1 channels evoked by 1-s voltage stimulus of –100 mV to 100 mV with 2 0mV increments from a holding potential at 0 mV. The pipette solution consisted of the following (in mM) : 145 CsCl, 5 EGTA, 10 HEPES, pH 7.3 adjusted with CsOH. The desired free calcium concentrations were obtained by adding $CaCl_2$ calculated by the MaxChealator (https://somapp.ucdmc.ucdavis.edu/). The bath solution contained (in mM) 145 NaCl, 1 $MgCl_2$, 10 Glucose, 10 HEPES, pH 7.3 adjusted with NaOH. Osmolarities of both bath and pipette solutions were measured by using Model 3320 osmometer (Advanced instruments) and adjusted to 310 mOsm with sucrose.

Cell surface biotinylation and western blot analysis

To test cell surface expression level of BEST1s, surface biotinylation was performed. HEK293T cells were transfected with each construct using Transporter 5™ Transfection Reagent and incubated for 1.5 days. PBS-washed cells were biotinylated using EZ-Link Sulfo-NHS-SS-Biotin for 20 min on ice. After quenching with 50 mM Glycine, pH 7.5, cells were lyzed in Lysis buffer (1% Triton X-100, 1X PBS, 1X Protease inhibitor cocktail). Biotinylated plasma membrane proteins were purified using NeutrAvidin Plus UltraLink Resin. After wash with Lysis buffer, purified proteins were eluted by 2X LDS sample buffer. Total and purified (Surface) proteins were separated on Bolt™ 4-12% Bis-Tris Plus Gel and transferred to PVDF membrane using iBlot 2 Transfer Stack. 10-250 ng antibodies/mL iBind Flex Solution were used for staining. Protein bands were visualized by Clarity Western ECL Substrate and images were acquired by ChemiDOC imaging system.

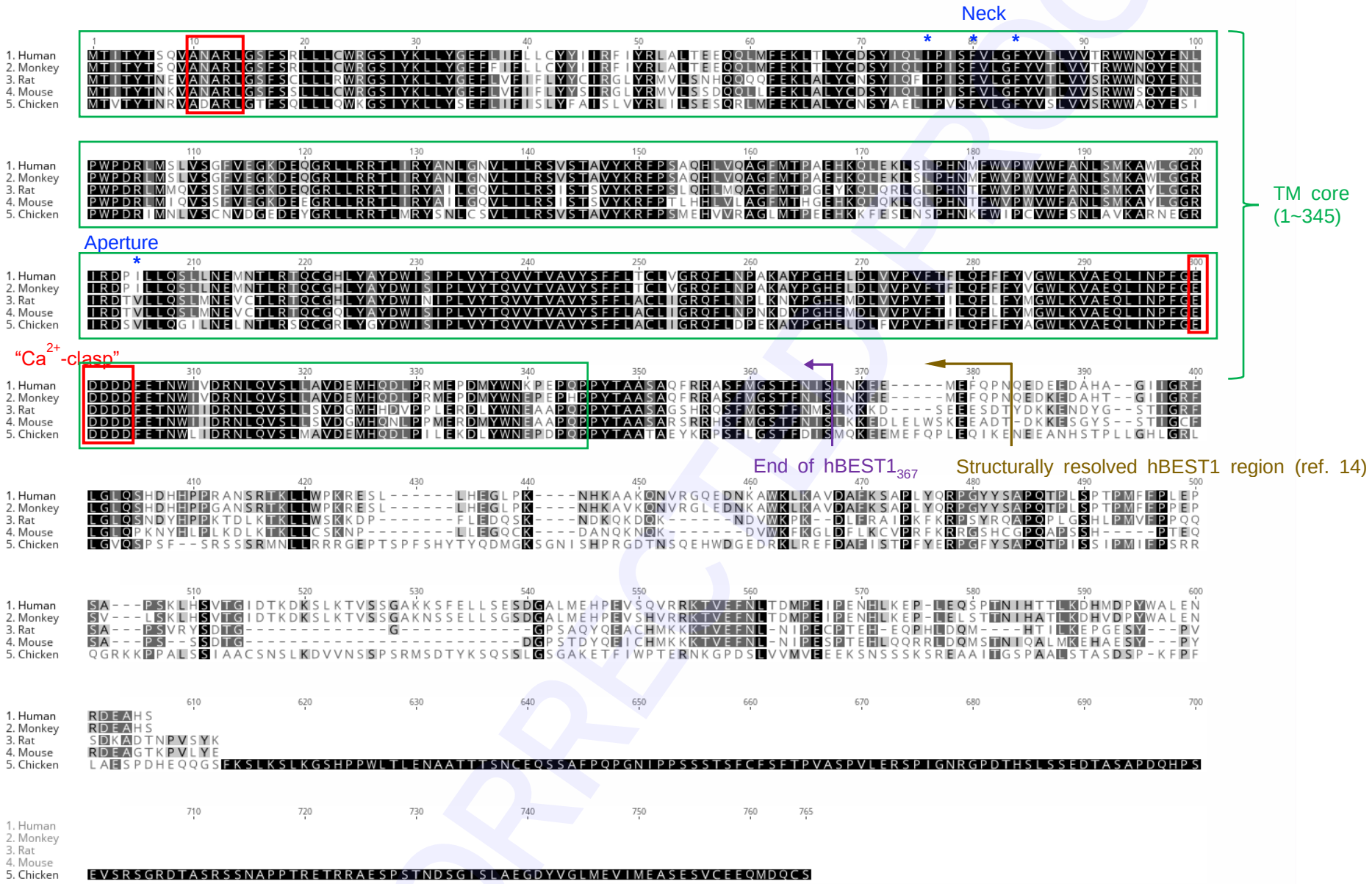

Fig. S1. Amino acid sequence alignment of BEST1 orthologs.

The amino acid sequences of BEST1 channel orthologs were aligned by using the Clustal O. The UniProt accession numbers of BEST1 orthologs are O76090 (human), Q6UY87 (monkey), Q6AYG9 (rat), O88870 (mouse), and E1C3A0 (chicken).The regions and residues described in the text are indicated by the colored text and marks.

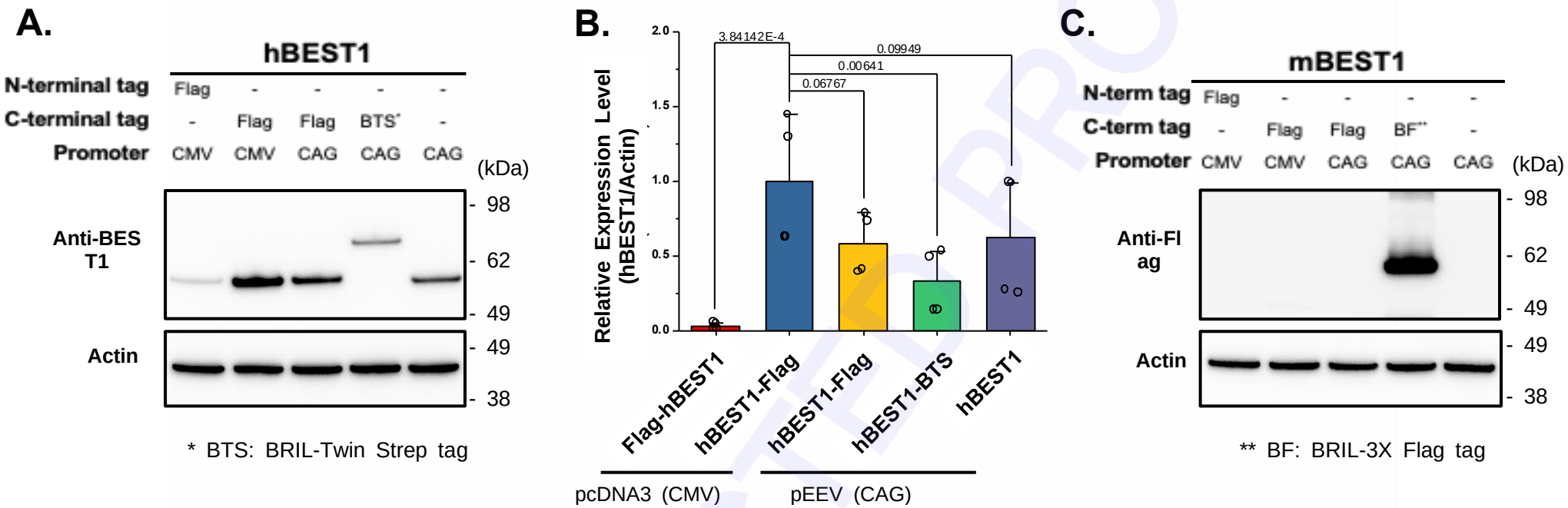

Fig. S2. Affinity-tags and their positions affect the expression of hBEST1 and mBEST1 in the CHO-K1 cells.

A. Representative western blot image of hBEST1 expressions tagged with the indicated affinity tags and position. Expression of each construct was driven by the CMV promoter (in pcDNA3 vector) or the CAG promoter (in pEEV vector). The hBEST1 proteins were detected by using anti-BEST1 antibody (ab2182). B. Quantification of hBEST1 protein expression level normalized to the density of actin. Data (mean ± s.e.m.) were produced by four independent transfections. Empty circles in the bar graphs indicate the values from the independent observations. One-Way ANOVA test was used for comparisons, and the appropriate P values are indicated in each graph. C. Representative western blot image of mBEST1 expressions tagged with the indicated affinity tags and position. The Flag-tagged mBEST1 proteins was detected by using anti-Flag (F1804) antibody.